Downloaded from orbit.dtu.dk on: Sep 13, 2024

DTU Library

NICER Discovers Spectral Lines during Photospheric Radius Expansion Bursts from 4U 1820−30: Evidence for Burst-driven Winds

Strohmayer, T. E.; Altamirano, D.; Arzoumanian, Z.; Bult, P. M.; Chakrabarty, D.; Chenevez, J.; Fabian, A. C.; Gendreau, K. C.; Guillot, S.; In 't Zand, J. J. M.

Total number of authors:
17

Published in:
Astrophysical Journal Letters

Link to article, DOI:
10.3847/2041-8213/ab25eb

Publication date:
2019

Document Version
Publisher's PDF, also known as Version of record

Link back to DTU Orbit

Citation (APA):
Strohmayer, T. E., Altamirano, D., Arzoumanian, Z., Bult, P. M., Chakrabarty, D., Chenevez, J., Fabian, A. C., Gendreau, K. C., Guillot, S., In 't Zand, J. J. M., Jaisawal, G. K., Keek, L., Kosec, P., Ludlam, R. M., Mahmoodifar, S., Malacaria, C., & Miller, J. M. (2019). *NICER* Discovers Spectral Lines during Photospheric Radius Expansion Bursts from 4U 1820−30: Evidence for Burst-driven Winds. *Astrophysical Journal Letters*, *878*(2), Article L27. https://doi.org/10.3847/2041-8213/ab25eb

General rights
Copyright and moral rights for the publications made accessible in the public portal are retained by the authors and/or other copyright owners and it is a condition of accessing publications that users recognise and abide by the legal requirements associated with these rights.

- Users may download and print one copy of any publication from the public portal for the purpose of private study or research.
- You may not further distribute the material or use it for any profit-making activity or commercial gain
- You may freely distribute the URL identifying the publication in the public portal

If you believe that this document breaches copyright please contact us providing details, and we will remove access to the work immediately and investigate your claim.

The Astrophysical Journal Letters, 878:L27 (11pp), 2019 June 20 https://doi.org/10.3847/2041-8213/ab25eb
© 2019. The American Astronomical Society. All rights reserved.

NICER Discovers Spectral Lines during Photospheric Radius Expansion Bursts from 4U 1820−30: Evidence for Burst-driven Winds

T. E. Strohmayer[1], D. Altamirano[2], Z. Arzoumanian[3], P. M. Bult[4], D. Chakrabarty[5], J. Chenevez[6], A. C. Fabian[7], K. C. Gendreau[3], S. Guillot[8,9], J. J. M. in 't Zand[10], G. K. Jaisawal[6], L. Keek[11], P. Kosec[7], R. M. Ludlam[12], S. Mahmoodifar[11], Christian Malacaria[13,14,16], and J. M. Miller[15]

[1] Astrophysics Science Division and Joint Space-Science Institute, NASA's Goddard Space Flight Center, Greenbelt, MD 20771, USA
[2] Physics & Astronomy, University of Southampton, Southampton, Hampshire SO17 1BJ, UK
[3] X-ray Astrophysics Laboratory, Astrophysics Science Division, NASA's Goddard Space Flight Center, Greenbelt, MD 20771, USA
[4] Astrophysics Science Division, NASA's Goddard Space Flight Center, Greenbelt, MD 20771, USA
[5] MIT Kavli Institute for Astrophysics and Space Research, Massachusetts Institute of Technology, Cambridge, MA 02139, USA
[6] DTU SpaceNational Space Institute, Technical University of Denmark, Elektrovej 327-328, DK-2800 Lyngby, Denmark
[7] Institute of Astronomy, Madingley Road, Cambridge CB3 0HA, UK
[8] CNRS, IRAP, 9 avenue du Colonel Roche, BP 44346, F-31028 Toulouse Cedex 4, France
[9] Université de Toulouse, CNES, UPS-OMP, F-31028 Toulouse, France
[10] SRON Netherlands Institute for Space Research, Sorbonnelaan 2, 3584 CA Utrecht, The Netherlands
[11] Department of Astronomy, University of Maryland College Park, MD 20742, USA
[12] Department of Astronomy, University of Michigan, 1085 South University Avenue, Ann Arbor, MI 48109-1107, USA
[13] NASA Marshall Space Flight Center, NSSTC, 320 Sparkman Drive, Huntsville, AL 35805, USA
[14] Universities Space Research Association, NSSTC, 320 Sparkman Drive, Huntsville, AL 35805, USA
[15] Department of Astronomy, University of Michigan, 1085 South University Avenue, Ann Arbor, MI 48109-1107, USA
Received 2019 April 19; revised 2019 May 29; accepted 2019 May 30; published 2019 June 14

Abstract

We report the discovery with the *Neutron Star Interior Composition Explorer* (*NICER*) of narrow emission and absorption lines during photospheric radius expansion (PRE) X-ray bursts from the ultracompact binary 4U 1820−30. *NICER* observed 4U 1820−30 in 2017 August during a low-flux, hard spectral state, accumulating about 60 ks of exposure. Five thermonuclear X-ray bursts were detected, of which four showed clear signs of PRE. We extracted spectra during the PRE phases and fit each to a model that includes a Comptonized component to describe the accretion-driven emission, and a blackbody for the burst thermal radiation. The temperature and spherical emitting radius of the fitted blackbody are used to assess the strength of PRE in each burst. The two strongest PRE bursts (burst pair 1) had blackbody temperatures of ≈0.6 keV and emitting radii of ≈100 km (at a distance of 8.4 kpc). The other two bursts (burst pair 2) had higher temperatures (≈0.67 keV) and smaller radii (≈75 km). All of the PRE bursts show evidence of narrow line emission near 1 keV. By coadding the PRE phase spectra of burst pairs 1 and, separately, 2, we find, in both coadded spectra, significant, narrow, spectral features near 1.0 (emission), 1.7, and 3.0 keV (both in absorption). Remarkably, all the fitted line centroids in the coadded spectrum of burst pair 1 appear systematically blueshifted by a factor of 1.046 ± 0.006 compared to the centroids of pair 2, strongly indicative of a gravitational shift, a wind-induced blueshift, or more likely some combination of both effects. The observed shifts are consistent with this scenario in that the stronger PRE bursts in pair 1 reach larger photospheric radii, and thus have weaker gravitational redshifts, and they generate faster outflows, yielding higher blueshifts. We discuss possible elemental identifications for the observed features in the context of recent burst-driven wind models.

Key words: radiation: dynamics – stars: neutron – X-rays: binaries – X-rays: bursts – X-rays: individual (4U 1820−30)

1. Introduction

Thermonuclear X-ray bursts provide unique opportunities to study the extreme physics of neutron stars. These bright X-ray events result from unstable burning in an accreted layer of light elements on the neutron star's surface. The strongly heated surface layers briefly shine brightly in the X-ray band, and as the radiation comes directly from the stellar surface, it provides important clues regarding neutron star structure and the nuclear burning on them (see Strohmayer & Bildsten 2006; Galloway & Keek 2017, for reviews). The continuum emission during bursts is broadly consistent with blackbody emission from the heated surface layers. A major focus of recent efforts has been to employ the observed spectra to constrain the stellar mass and radius (Lewin et al. 1993). The basic idea is to measure an X-ray flux, F_x, and color temperature, $T_{\rm col}$, and then use an appropriate atmosphere model to convert the color temperature to an effective temperature, $T_{\rm eff}$. One can then, in principle, infer an assumed spherical emission area from the Stefan Boltzmann law, $L = 4\pi d^2 F_x = 4\pi R^2 \sigma T_{\rm eff}^4$, where d and R are the source distance and photospheric radius, respectively. For bursts that reach the Eddington luminosity, an additional constraint is available, as this quantity depends only on the stellar mass, radius, and the composition of the atmosphere. A full treatment must also account for the significant gravitational redshift from the neutron star surface, as well as any special relativistic effects associated with the potentially rapid spin of its surface. Substantial efforts have been made by a number of research groups over the past decade to carry out this program (see, for example, Özel 2006; Steiner et al. 2010;

[16] NASA Postdoctoral Fellow.

Güver et al. 2016; Nättilä et al. 2017, and references therein). While very promising, significant uncertainties remain in interpreting such observations. These can be illustrated with a few rhetorical questions: how accurate is the atmosphere model, in particular its composition? Are other emission components, such as, for example, reprocessed emission from an accretion disk, present in the observed spectrum? How accurately are the distance, flux, and color temperature known?

Another way to obtain constraints on the stellar mass and radius is to infer a surface gravitational redshift, $z = (E_0 - E)/E$, by observing a spectral feature; a line or edge at energy E that originates from the stellar surface, of a known, rest-frame transition with energy E_0. A constraint on the mass-to-radius ratio, the "compactness," M/R, then follows from the relation $1 + z = (1 - 2GM/c^2R)^{-1/2}$. While perhaps conceptually simpler than correctly interpreting observed continuum spectra, questions remain. Is the line identification secure? Is the emission site at the stellar surface, or some other altitude or location? Perhaps most fundamental of all is that it has been very difficult to reliably identify *any* surface spectral features in X-ray burst spectra.

There were some early claims of absorption line detections from the bursters 4U 1636−536, 4U 1608−522, and EXO 1747−214 based on data from *Tenma* and *EXOSAT* (Waki et al. 1984; Nakamura et al. 1988; Magnier et al. 1989), but subsequent observations with *ASCA*, *RXTE,* and *BeppoSAX* did not tend to confirm these initial reports. There has also been a recent report based on *NuSTAR* observations of GRS 1741.9 −2853 of an absorption line at 5.46 ± 0.1 keV during an X-ray burst from this object (Barrière et al. 2015). However, the reported significance of the line was rather modest (1.7σ). Observations of two superbursts, from 4U 1820−30 and 4U 1636−536, with the *RXTE* Proportional Counter Array (PCA), clearly show emission features in the Fe K band that have been successfully modeled as burst thermal emission reprocessed (reflected) by the accretion disk (Strohmayer & Brown 2002; Keek et al. 2014a, 2014b). While these features provide an exciting view of the interaction of the burst flux with the accretion disk (Ballantyne & Strohmayer 2004; Fragile et al. 2018), it seems highly likely that they do not originate at the stellar surface.

Cottam et al. (2002) reported on a set of narrow absorption lines in the coadded, high-resolution spectra of 28 bursts from EXO 0748−676 observed with the *XMM-Newton* Reflection Grating Spectrometer. They argued that these features could be associated with transitions of Fe XXV, Fe XXVI, and O VIII at a consistent surface redshift of $1 + z = 1.35$. Unfortunately, subsequent observations did not confirm these lines, and the likely stellar spin frequency was determined to be 552 Hz (Galloway et al. 2010), substantially higher than the 45 Hz value that was initially reported for the source (Villarreal & Strohmayer 2004). The higher spin rate implies rotational broadening that would be incompatible with the narrow absorption lines initially claimed (Lin et al. 2010). Additionally, detailed model atmosphere calculations by Rauch et al. (2008) did not confirm the line identifications proposed by Cottam et al. (2002). Whether the lines are real or not remains controversial.

More recently, there have been reports of absorption edges being detected during X-ray bursts. in't Zand & Weinberg (2010) reported evidence from *RXTE*/PCA data for edges during so-called "superexpansion" bursts from 4U 0614+091, 4U 1722−30, and 4U 1820−30. These are bursts with powerful photospheric radius expansion (PRE) phases, that very likely drive outflows (in't Zand et al. 2012; Yu & Weinberg 2018). The edge energies were in the 5–12 keV range, and were detected after the strong, initial expansion phase. Degenaar et al. (2013) reported the detection with the *Swift*/XRT of a 1 keV emission line, as well as Fe-K band absorption features (lines and edges) in an energetic, intermediate-duration thermonuclear burst from the ultracompact accreting millisecond X-ray pulsar (AMXP) IGR J17062 −6143 (Strohmayer et al. 2018). They suggested the 1 keV emission line could be associated with Fe-L shell transitions from the irradiation of cold gas by the burst, or alternatively, the $1s$–$2p$ Lyα transition of Ne X could also account for the observed line energy.

Kajava et al. (2017) reported evidence for absorption edges at decreasing energies between 8 and 7.6 keV in a powerful He flash from the AMXP HETE J1900.1−2455. Like in't Zand & Weinberg (2010), they argue that these features are associated with metals—the ashes of the thermonuclear burning—that have been dredged up by the vigorous convection initiated by such bursts (Weinberg et al. 2006). Kajava et al. (2017) identified the features in HETE J1900.1−2455 with the 9.28 keV photoionization edge of hydrogen-like Fe ions, but redshifted from the stellar surface to the observed energies. The variation in observed edge energy is attributed to variation in the vertical location of the photosphere. Based on this the authors estimate $1 + z \approx 1.2$, which is roughly consistent with the redshift expected from a neutron star with $M = 1.4\,M_\odot$ and $R = 12$ km. Li et al. (2018) also claimed an absorption edge is present during a PRE burst from GRS 1747−312 observed with the *RXTE*/PCA. They reported evolution of the absorption edge energy from 9.45 to ≈6 keV through the PRE phase, and then to ≈8 keV in the cooling tail. They attributed the shift from 9.45 to 8 keV to gravitational redshift of the hydrogen-like Ni photoionization edge between the neutron star surface and the expanded photosphere during PRE. We note that this is the same burst for which in't Zand et al. (2003) reported evidence of a broad emission feature at 4.8 keV during the PRE phase, so interpretation of the apparent features in this burst as edges may not be unique.

Many of the reported detections of spectral features in X-ray bursts to date have been made with data from instruments with relatively poor resolution, such as *RXTE*'*s* PCA, which has a ≈20% resolution at 6 keV. Higher-resolution detectors have typically suffered from some technical problems when observing bright X-ray bursts. The high count rates mean that CCD detectors suffer pile-up or relatively higher backgrounds are present when they must be clocked at high rates. Whereas dispersive spectroscopy with either *Chandra* or *XMM-Newton* generally mitigates any pile-up, these instruments bring relatively modest effective area to bear on the brief intervals for which bursts are bright. Fortunately, *Neutron Star Interior Composition Explorer* (*NICER*'*s*) X-ray Timing Instrument (XTI) brings a CCD-like spectral resolution (≈80 eV at 1 keV), and substantial, pile-up-free effective area to observations of X-ray bursts. Moreover, *NICER*'*s* bandpass extends down to 0.2 keV, which is ideal for observing the soft-X-ray expansion phases of PRE bursts. With the recently reported detections of edge features in such bursts, we aim to leverage *NICER*'s unique capabilities to search for similar features.

Table 1
X-Ray Bursts from 4U 1820 Observed by *NICER*

Number	ObsID	Start Time MJD (TT)	Date YYYY MM DD	$kT_{\rm PRE}$ (keV)	$R_{\rm PRE}$ (km)
1	1050300108	57994.37115	2017 Aug 29	0.573 ± 0.025	103 ± 9
2	1050300108	57994.46169	2017 Aug 29	NA	NA
3	1050300109	57995.22281	2017 Aug 30	0.619 ± 0.026	102 ± 7
4	1050300109	57995.33890	2017 Aug 30	0.675 ± 0.030	78 ± 6
5	1050300109	57995.60332	2017 Aug 30	0.664 ± 0.035	72 ± 7

Note. Assigned number, observation ID, burst start time, date of observation, blackbody temperature (keV), and derived photospheric radius (km, at 8.4 kpc).

In this paper we report results of *NICER* observations of thermonuclear X-ray bursts from 4U 1820−30 (hereafter, 4U 1820), which reveal both emission and absorption features during their PRE phases. 4U 1820 is a well-known, ultracompact accreting neutron star binary with an 11.4 minute orbital period. The system was one of the first discovered to produce thermonuclear X-ray bursts (Grindlay et al. 1976). Its compact nature requires a low-mass degenerate dwarf donor (Rappaport et al. 1987), and helium is likely the most abundant burst fuel (Haberl et al. 1987; Bildsten 1995; Cumming 2003).

The paper is organized as follows. We first briefly describe the observations and the general properties of the observed bursts. We then discuss our spectral analysis and the evidence for an emission line at 1 keV, and absorption lines at 1.7 and 3.0 keV in the PRE phases of these bursts. We also show that there is a systematic energy shift present in the coadded spectra of the pair of the strongest PRE bursts, compared to those in the burst pair with weaker PRE. We then discuss several scenarios for the origin of the line features, and provide possible elemental identifications. We also explore the idea that some of the observed energy shift is related to a gravitational redshift, a wind-induced blueshift, or perhaps both. We conclude with a brief summary and discussion of the implications for models of burst winds and future efforts to probe their composition, energetics, and formation.

2. *NICER* Observations

NICER is an X-ray observatory operating on the *International Space Station* (*ISS*). It provides low-background, high-throughput ($\approx$1900 cm^2 at 1.5 keV), high time resolution observations across the 0.2–12 keV X-ray band (Gendreau et al. 2012). *NICER* observed 4U 1820 in 2017 August, accumulating about 60 ks of exposure as part of a science team program with a major goal to detect X-ray bursts and search for spectral features in them. These observations were triggered by the entry of the source into a low flux and hard spectral state in which it is known to produce bursts (Keek et al. 2018). These data were processed using the NICERDAS (V004) software, and standard filtering and cleaning were applied. This involves excluding all data where the pointing offset is $>54''$, the dark Earth limb angle is $<30°$, the bright Earth limb angle is $<40°$, and the *ISS* was inside the South Atlantic Anomaly (SAA). We employed version v1.02 of the *NICER* response functions in our analysis.

2.1. Burst Light Curves

Five bursts were observed during this campaign (see Table 1). We note that detailed, time-resolved spectroscopy of burst 1 was reported in Keek et al. (2018), and it is not our goal here to reproduce such an analysis for all the observed bursts. We began by extracting light curves for each burst in several energy bands; 0.2–1 keV (soft), 2–10 keV (hard), and the full band 0.2–10 keV. Figure 1 shows the resulting soft and hard band light curves for bursts 1 (top left), 3 (top right), 4 (bottom right), and 5 (bottom left), all of which show evidence for PRE, in that the soft band rate (black curves) peaks while there is a correlated drop in the hard band rate (red curves). Burst 2 is "anomalous" in this regard. The hard band rate is actually larger than that in the soft band, and there are correlated drops in both rates during the burst rise. This behavior is suggestive of an additional absorption component present during this burst. Because it lacks a clear signature of PRE we did not consider it in the spectral analysis reported here. We will explore this interesting burst elsewhere. In Figure 2 we show the light curves of all five bursts in the full band (0.2–10 keV). The caption gives the color code to identify the bursts. We approximately aligned the rise times for display purposes so that the profiles can be compared. The cyan curve is burst 2, and the prominent dip after the initial rise is apparent.

2.2. Single-burst Spectra

Guided by the results of Keek et al. (2018) we began by extracting spectra during the PRE phases for each burst. We identified the interval where the 2–10 keV band light curve peaks and extracted spectra for 0.7 s from this point for each burst. This exposure value approximately encompasses the lowest-temperature portion of the PRE phase (see Keek et al. 2018, Figure 3), and these intervals are marked in Figure 1 by the vertical dashed lines. We regrouped the spectra by combining every three successive, native energy (PI) channels, and we also applied a normalization factor derived from spectral fits to data from the Crab Nebula. See Ludlam et al. (2018) for a discussion of this procedure, which provides a way to reduce the influence of the strongest remaining unmodeled residuals in the *NICER* response function. We then fit each spectrum in the band 0.3–7 keV with a two-component model comprising a Comptonized component for the persistent emission and a blackbody for the thermal burst flux. We note that the *NICER* background is always negligible in this energy band for these bright source spectra. In XSPEC this model has the form, *TBabs*(nthcomp + bbodyrad)*. See Życki et al. (1999) for a description of the *nthcomp* model.

The parameters of the *nthcomp* (persistent) component are qualitatively similar for all bursts. For example, for burst 3 we find, $\Gamma = 2.2 \pm 0.1$, $kT_{\rm bb} = 0.14 \pm 0.03$ keV, and a normalization of 7.9 ± 1.1 (errors are 1σ). The normalization is defined as the photon flux (with units, cm^{-2} s^{-1} keV^{-1}) at 1 keV. These spectra are not sensitive to the electron temperature, kT_e, in this model, so for all fits we held it fixed

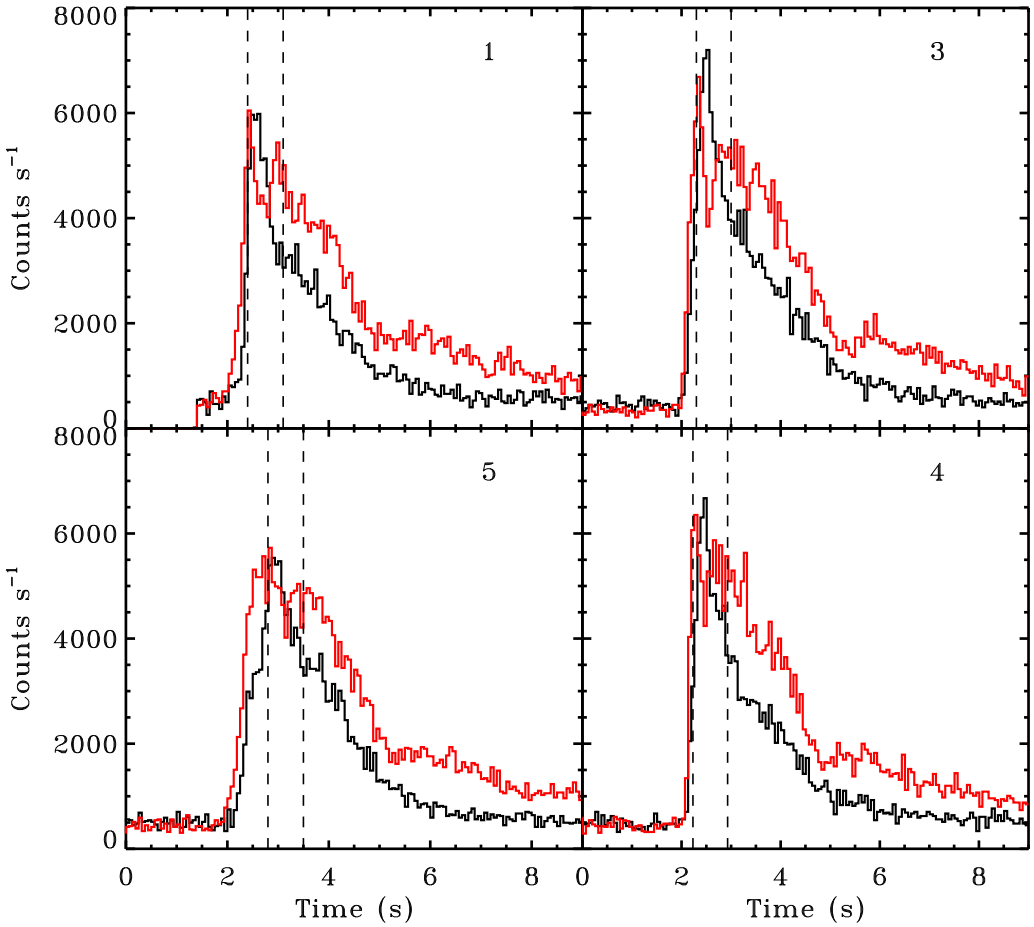

Figure 1. Light curves of four PRE X-ray bursts from 4U 1820 observed with *NICER*. Count rates computed in 1/16 s intervals in the 0.2–1.0 keV (black) and 2.0–10.0 keV (red) bands are shown. The vertical dotted lines mark the intervals used to extract PRE phase spectra. Clockwise from upper left, the four panels correspond to bursts 1, 3, 4, and 5 (see Table 1).

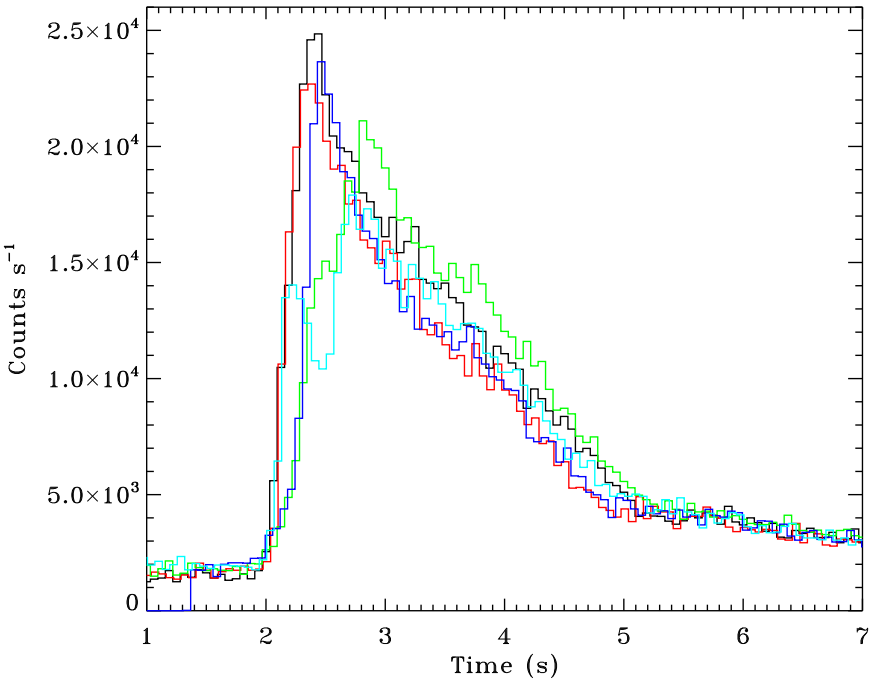

Figure 2. Light curves of all five X-ray bursts from 4U 1820 observed with *NICER*. Count rates computed in 1/16 s intervals in the full *NICER* band (0.2–10.0 keV) are plotted. For comparison purposes, the start times have been approximately aligned. The different colors correspond to the following bursts: 1 (blue), 2 (cyan), 3 (black), 4 (red), and 5 (green). Burst 2 (cyan) is "anomalous" in that it shows a significant drop in count rate in both the soft and hard bands, and does not show evidence of PRE.

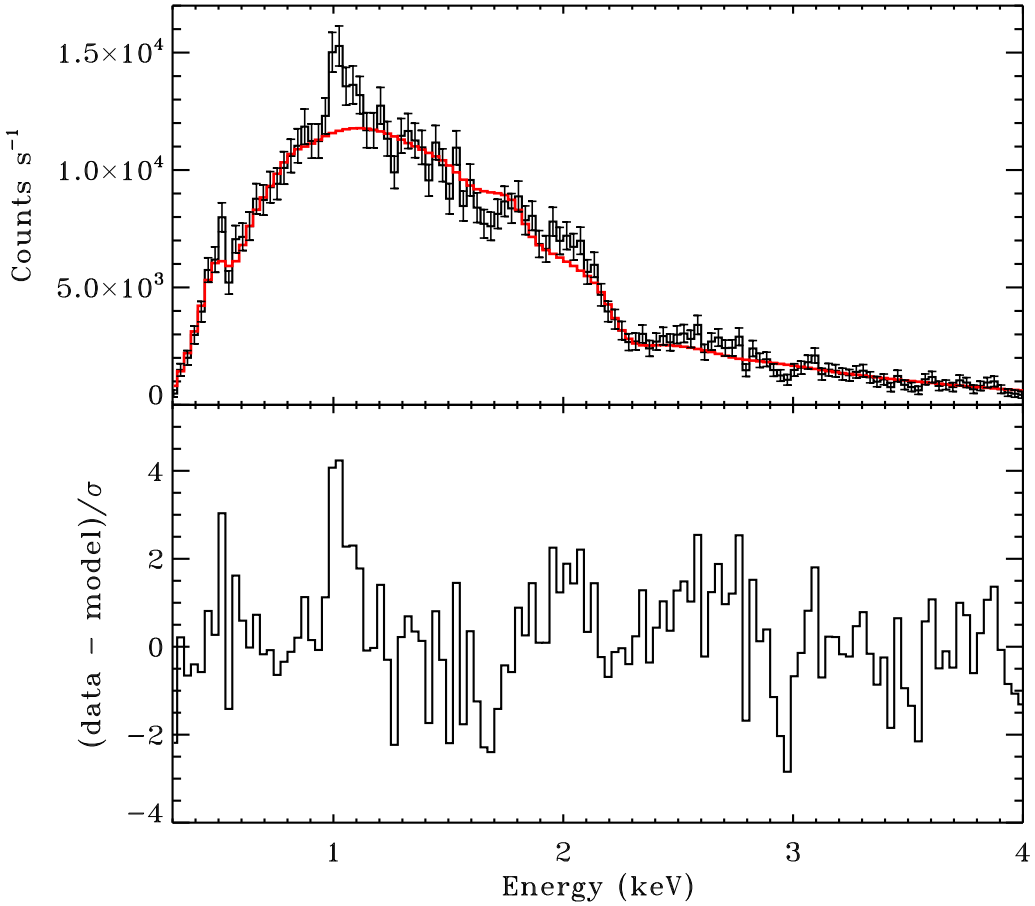

Figure 3. X-ray count rate spectrum extracted during the PRE phase for burst 3. The top panel shows the observed count rate as a function of energy. The red curve is the best-fitting continuum model. The fit residuals, in units of (data—model)/σ, are shown in the bottom panel. Excess emission is evident near 1 keV. See Section 2.2 for additional details.

at 8 keV. We left all other parameters describing the *nthcomp* component free to vary, but we note that the fitted parameter values describing the spectral shape are all qualitatively similar to those derived from fitting the pre-burst (persistent) emission with the same model. The derived blackbody temperature and spherical emitting radius characterizing the PRE phase do show significant variations burst to burst, and these are listed in Table 1 for each burst.

The above continuum model provides a reasonable, qualitative fit to the PRE phase spectra, but there are substantial residuals evident in the spectra. The most prominent of these is an excess near 1 keV in all of the bursts, but it is most obvious in bursts 1 and 3. As an example, we show in Figure 3 the PRE phase spectrum extracted for burst 3, where one can see excess emission above the continuum near 1 keV. Adding a Gaussian component to model this feature results in an improvement in χ^2 of 34.8. The fitted line centroid is 1.04 ± 0.01 keV, and an estimate of the significance, defined as the ratio of the line normalization to its 1σ uncertainty, is 6.1. The equivalent width is 47 eV. The line is unresolved in the sense that we only find an upper limit to its intrinsic width of ≈70 eV (90% confidence). The observed width, however, is consistent with *NICER*'*s* measured spectral resolution at 1 keV.

2.3. Coadded Spectra

As noted above, a similar 1 keV excess is apparent in the PRE spectra from each of the bursts, but with somewhat varying strength. Motivated by this we coadded bursts in pairs to improve the signal-to-noise ratio. In order to combine bursts that are most similar to one another, we were guided by their spectral properties inferred during the PRE phase (see Table 1). The bursts with the lowest PRE temperatures and the largest photospheric radii are bursts 1 and 3. Bursts 4 and 5 have higher temperatures and smaller radii that are consistent within the uncertainties. The burst pairs that are most similar to each other are therefore bursts 1 and 3 (pair 1), and bursts 4 and 5 (pair 2). We thus created two new spectra by coadding the single-burst spectra within each pair.

We fit the same model described above to both coadded spectra. Figure 4 shows the spectrum from pair 1, where the red curve (top) represents the best-fitting continuum model. It is consistent with the individual results for bursts 1 and 3. We find for the *nthcomp* component $\Gamma = 1.98 \pm 0.06$, $kT_{\rm bb} = 0.130 \pm 0.02$ keV, and a normalization of 7.75 ± 0.7. For the burst blackbody component we obtain $kT_{\rm PRE} = 0.615 \pm 0.018$ keV, and $R_{\rm PRE} = 95.4 \pm 5$ km, which are also consistent with the individual results for bursts 1 and 3. We find for $N_{\rm H}$ a value of $0.17 \pm 0.03 \times 10^{22}$ cm^{-2}, which is consistent with the value reported by Güver et al. (2010).

One can see in Figure 4 that the excess at 1 keV is now strikingly evident, and there is also now a clearer indication for a pair of absorption features near 1.7 and 3 keV. We note that the spectrum of burst 3 alone (see Figure 3) shows tentative indications for these features, but they stand out more clearly in the coadded spectrum. To assess these features further, we

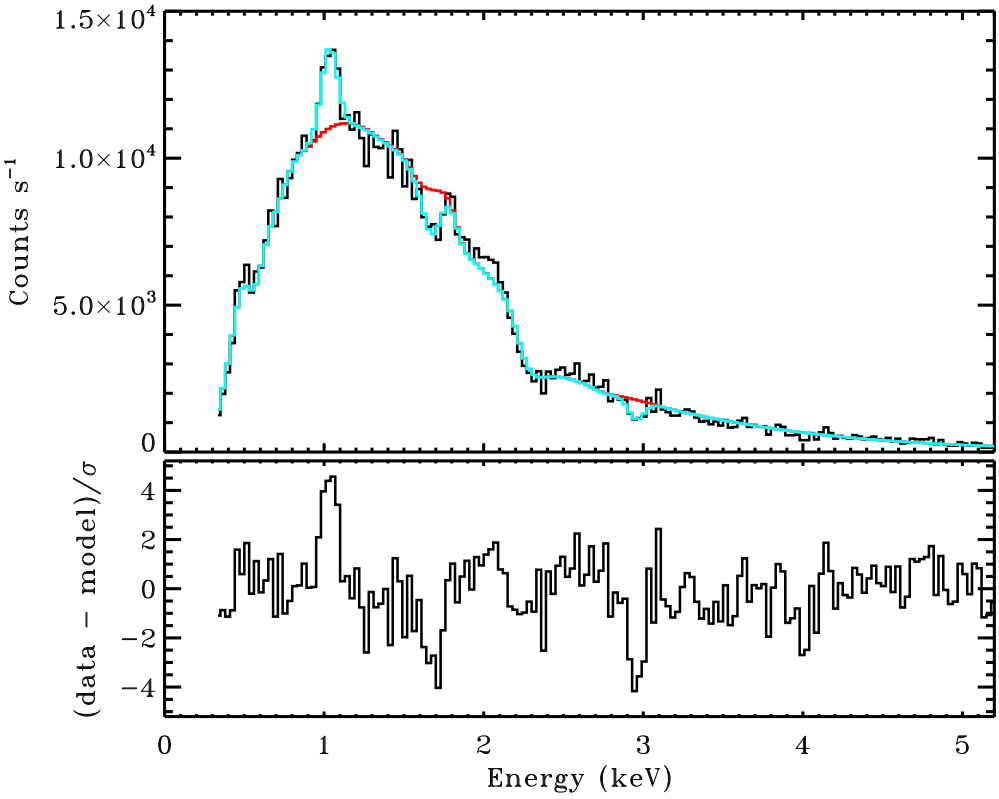

Figure 4. Coadded count rate spectrum of the PRE phases of bursts 1 and 3 (burst pair 1). The top panel shows the observed count rate as a function of energy. The red curve is the best-fitting continuum model, and the cyan curve is the best-fitting model including the continuum and three, narrow Gaussian line components at 1, 1.7, and 3 keV. The fit residuals, in units of (data—model)/σ, for the best-fitting model with the line normalizations set to zero, are shown in the bottom panel. The excess emission is clearly evident near 1 keV, and a pair of absorption lines are indicated near 1.7 and 3 keV. See Section 2.3 for additional details.

added three narrow Gaussians to the model. Including the line components dramatically improves the overall fit, and is shown as the cyan curve in Figure 4. Table 2 summarizes the results of the fitted line components. We find strong evidence for the presence of three lines at 1.043 ± 0.008, 1.689 ± 0.012, and 2.964 ± 0.014 keV. The strongest, at 1 keV appears in emission, and the others in absorption. As an estimate of the significance of each line we quote the ratio of the fitted line normalization to its 1σ uncertainty. All the lines are above 5σ, and the 1 keV feature is at 7σ. The bottom panel of Figure 4 shows the line residuals using the best-fitting model, but with the line normalizations set to zero. The overall spectral fit including the three line components has $\chi^2 = 279$ for 227 degrees of freedom (dof), which is formally a bit high; however, the most substantial remaining residuals near 0.5–0.6 and 2.0–2.4 keV, are consistent with energy ranges with the most significant unmodeled residuals in the *NICER* response function (Ludlam et al. 2018). We emphasize that there are no comparably strong, nor narrow, unmodeled residuals at the centroid energies inferred for the three fitted line components. Thus, we think that a significant part of the excess χ^2 in our fits is likely associated with remaining uncertainties in the *NICER* response function. Fortunately, this will be testable, as the *NICER* response model is refined over time.

We carried out the same fitting procedure for burst pair 2, with the corresponding results summarized in Figure 5. Remarkably, there is evidence for line features near the same energies as for burst pair 1, with the emission feature near 1 keV being, again, the clearest excess (compare Figures 4 and 5). For the *nthcomp* continuum, in the absence of any line components, we find

Table 2
Spectral Results for Line Components

Parameter	Burst Pair 1	Burst Pair 2
Centroid Energy (keV)	1.043 ± 0.008	1.000 ± 0.008
Line Norm (ph)	0.314 ± 0.045	0.266 ± 0.045
Line width (keV)	0.06	0.07
$\Delta\chi^2$	61.6	44.6
σ	7.0	5.9
Equivalent width (eV)	33	27
Centroid Energy (keV)	1.689 ± 0.012	1.592 ± 0.014
Line Norm (ph)	-0.125 ± 0.023	-0.097 ± 0.016
Line width (keV)	0.07	0.07
$\Delta\chi^2$	29.1	22.6
σ	5.5	4.7
Equivalent width (eV)	23	21
Centroid Energy (keV)	2.964 ± 0.014	2.846 ± 0.0164
Line Norm (ph)	-0.090 ± 0.0146	-0.079 ± 0.0159
Line width (keV)	0.06	0.07
$\Delta\chi^2$	38.4	24.5
σ	5.9	5.0
Equivalent width (eV)	50	39

Note. Results for Gaussian line component parameters from fits to the coadded spectra of burst pairs 1 and 2. In each case three Gaussian line components have been fitted. The widths are 90% confidence upper limits, as all the lines are unresolved. The value σ is an estimate of the significance of the line, and is defined as the ratio of the line normalization to its uncertainty (1σ).

$\Gamma = 1.88 \pm 0.05$, $kT_{\rm bb} = 0.123 \pm 0.03$ keV, and a normalization of 7.82 ± 0.6. For the burst blackbody component we obtain $kT_{\rm PRE} = 0.675 \pm 0.026$ keV, and $R_{\rm PRE} = 71.6 \pm 5$ km, which

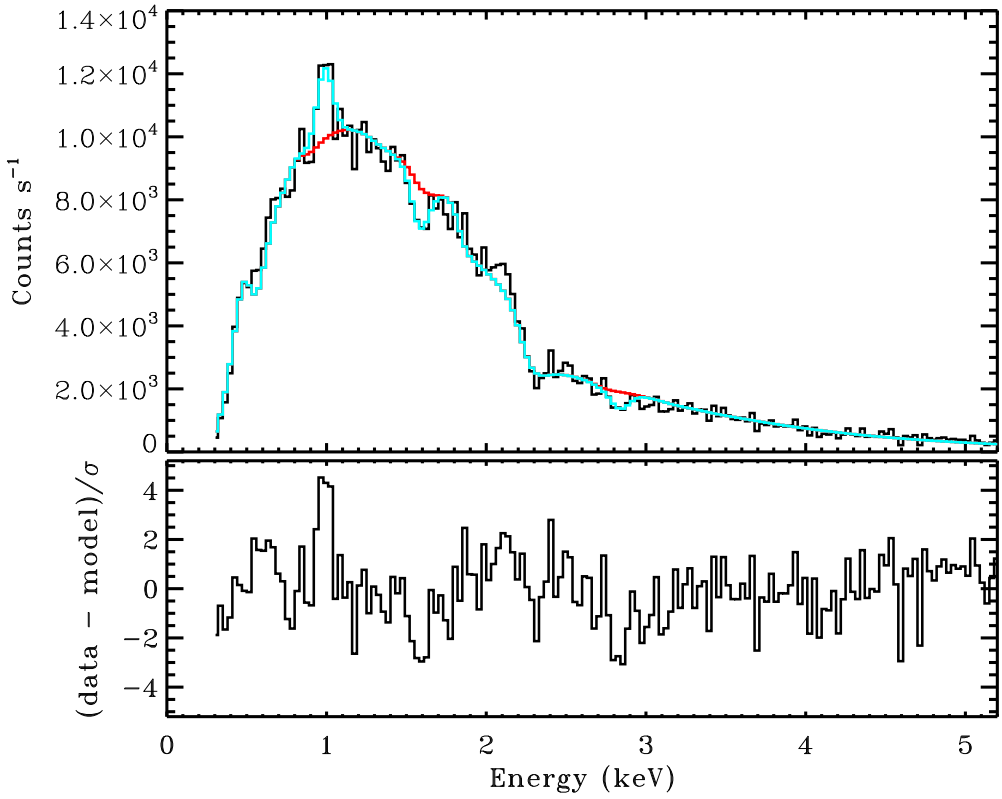

Figure 5. Coadded count rate spectrum of the PRE phases of bursts 4 and 5 (burst pair 2). Other details are the same as in Figure 4. Features similar to those evident in burst pair 1 (Figure 4) are also apparent in this spectrum. See Section 2.3 for further details.

are consistent with the individual results for bursts 4 and 5. The overall fit is of a similar quality to that of burst pair 1, but with a slightly higher $\chi^2 = 295$ for 227 dof. In burst pair 2 the line features appear slightly weaker. This is evident in the somewhat smaller σ values (Table 2). Nevertheless, they are all at values greater than 4.7. The fact that similar features are apparent in both independent sets of burst spectra is a very strong indication that they are real astrophysical features.

To further explore the link between the identified line features and the PRE phase in which they are found, we extracted spectra from additional time intervals after the strong PRE phase to see if there is any evidence that the lines may persist throughout the bursts. We found no indication that the absorption lines persist beyond the strong PRE phases described above, but we found some indication for a persistence of the 1 keV emission line beyond the PRE phase in burst pair 1. As a demonstration of this we show results for spectra accumulated for 1 s intervals *after* the PRE phases in which the lines were identified, as well as 4 s intervals later in the decaying tail. We call these the "post-PRE" and "tail" spectra, respectively. For consistency we coadded these spectra by burst pairs in the same way as described above for the PRE phases, and we fit the same model as employed for the PRE phases. Residuals to the fits for the post-PRE (top) and tail (bottom) spectra are shown for both burst pairs in Figure 6. As is rather clear from Figure 6 (bottom), the tail spectra show no evidence for comparable line features like those seen in the PRE phases. On the other hand, for burst pair 1 there is some evidence for a persistence of the 1 keV emission feature into the post-PRE phase (see Figure 6, top). Including the 1 keV line feature to the fit in this case gives a significance of 4.2σ, measured as the ratio of the fitted line normalization to its 1σ uncertainty, and an equivalent width of 21 eV. The line centroid energy is consistent with that measured in the PRE phase. There are no comparable indications for persistence of the absorption features, and the results suggest these are rather clearly linked to the strong PRE phase. Finally, we also analyzed a 1200 s exposure of the persistent emission prior to burst 3. There are no comparable line features evident in that spectrum as well.

Looking more closely at the measured line centroids and uncertainties, there is a very significant, systematic shift when comparing the line energies in burst pair 1 with those in pair 2 (see Table 2). All of the energy centroids measured in burst pair 2 are systematically lower. To explore this further, we computed the ratios of the line energy centroids in burst pair 1 to those in pair 2, and their uncertainties, and fit the values to a constant, s_0. The results are shown in Figure 7. The line energy ratios are statistically consistent with a constant value of $s_0 = 1.046 \pm 0.006$, suggesting that the lines from burst pair 2 are redshifted relative to those of pair 1. Figure 8 shows the fit residuals for both coadded spectra using the best-fitting model with the line component normalizations set to zero. The top panel shows the residuals for burst pair 1 (black) and 2 (red), and the systematic energy shift is readily apparent. If we shift the residuals for pair 2 by the best-fit value of $s_0 = 1.046$, and then average them with those of pair 1, we obtain the "shift and add" residuals in the bottom panel.

3. Interpretation and Discussion

We have presented strong evidence from *NICER* observations for the existence of narrow spectral lines during the PRE phases of X-ray bursts from 4U 1820. The strongest feature we

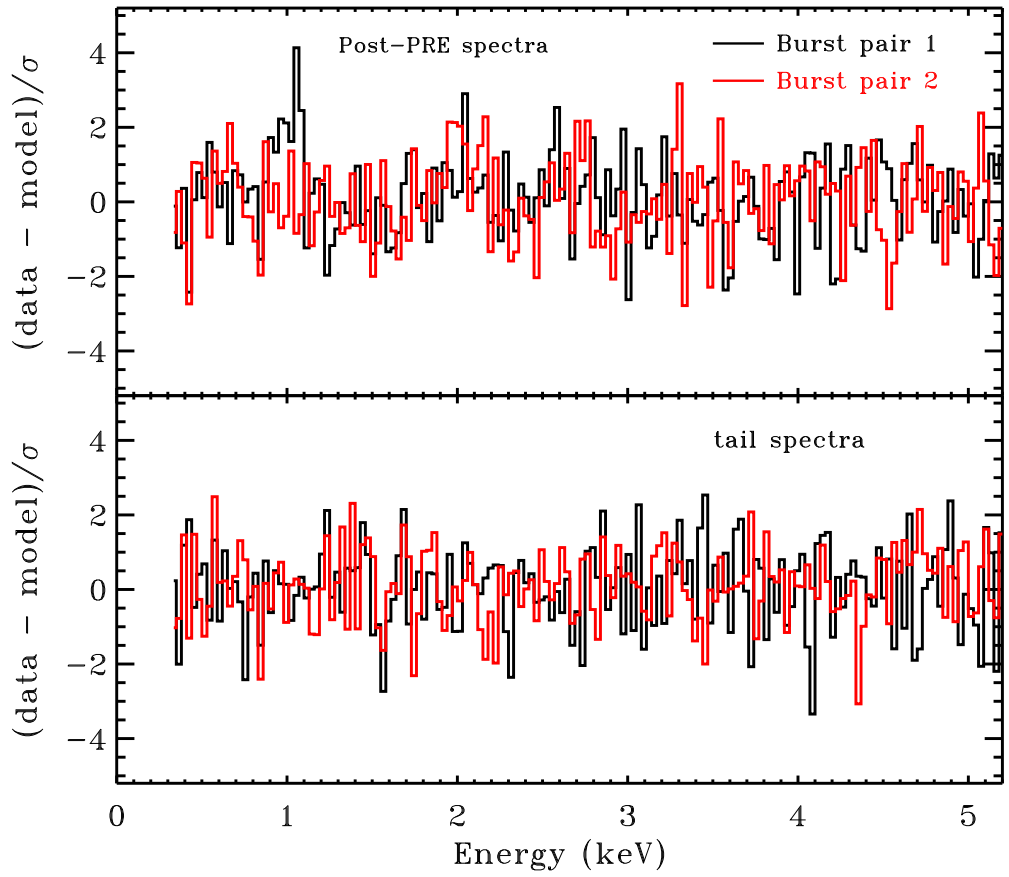

Figure 6. Fit residuals obtained from the post-PRE (top) and tail (bottom) intervals for both burst pairs 1 (black) and 2 (red) are shown in units of (data—model)/σ. The tail spectra show no evidence for line features, and only the post-PRE phase for burst pair 1 shows some evidence for the 1 keV emission feature.

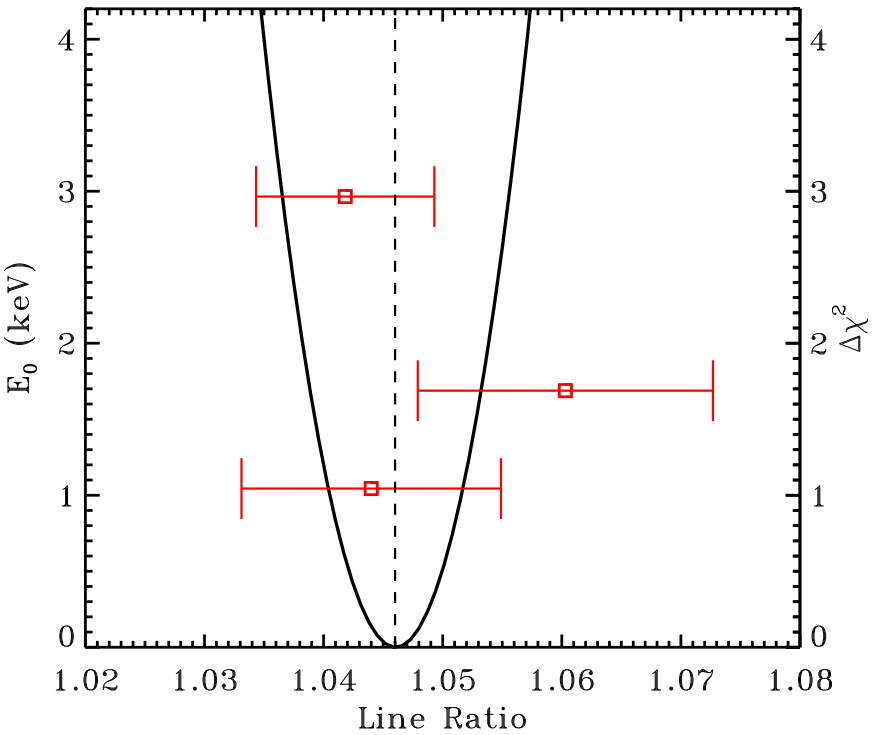

Figure 7. Measured line energy ratios and uncertainties of the 1, 1.7, and 3 keV line features obtained from burst pairs 1 and 2 (red symbols). Also shown, on the right vertical axis, are the $\Delta\chi^2$ values for a single-parameter, constant line ratio fit (solid black curve). The best-fitting value of the line energy ratio, $s_0 = 1.046 \pm 0.006$ (1σ, $\Delta\chi^2 = 1$) is marked by the vertical dashed line. A constant ratio is a good statistical description of the three observed line energy ratios.

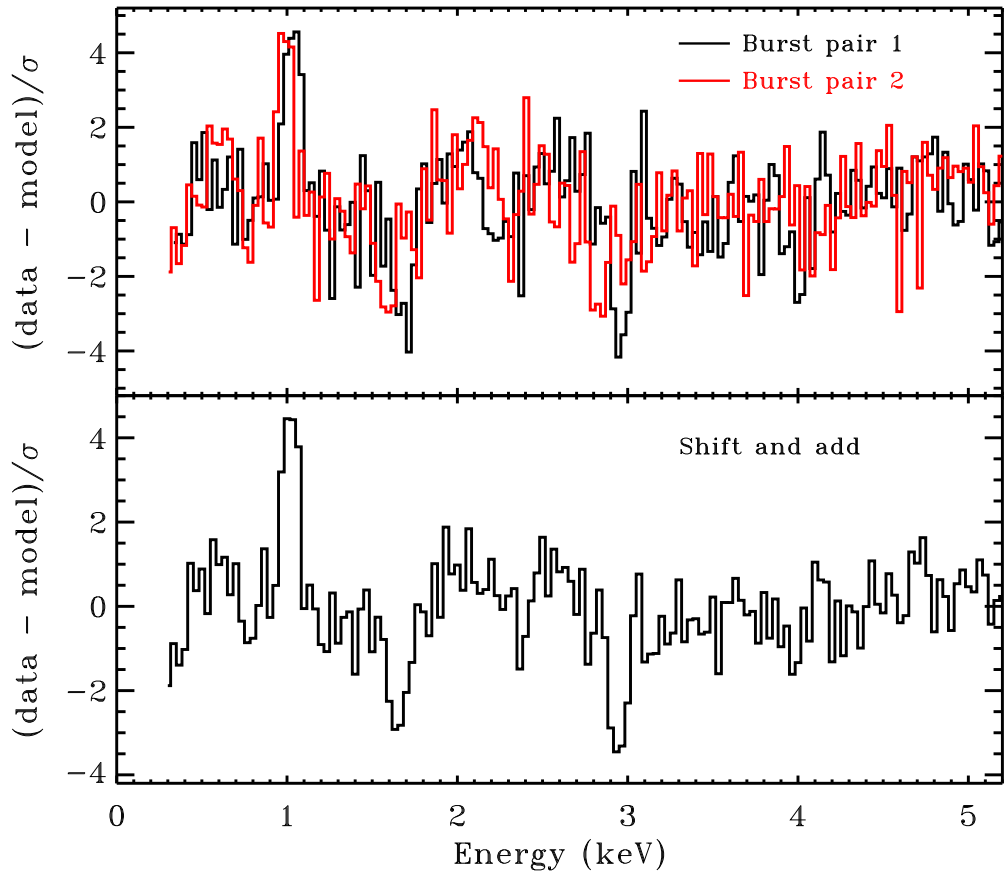

Figure 8. Fit residuals for both burst pairs 1 (black) and 2 (red) shown in units of (data—model)/σ (top). Here, the plotted residuals were obtained from the best-fitting model after setting the fitted line normalizations to zero. Also shown are the average ("shift and add") residuals when the burst pair 2 spectrum is shifted in energy by the best-fitting constant line ratio of 1.046 and averaged (see Figure 7 and Section 2.3).

identify is the emission line near 1 keV. The properties of this feature appear rather similar to the 1 keV emission line reported by Degenaar et al. (2013) in an energetic, intermediate-duration burst from the ultracompact AMXP IGR J17062−6143. 4U 1820 is now the second system to show such a line in emission, and it is intriguing that both objects are ultracompact systems likely accreting helium-rich fuel (Cumming 2003; Strohmayer et al. 2018). Interestingly, Degenaar et al. (2013) reported shifts in the line centroid energy during the IGR J17062−6143 burst that are at about the same level that we find for the 4U 1820 PRE bursts (≈1.0–1.044 keV). These authors argued that the 1 keV line could be due to Fe L shell transitions from relatively cool irradiated gas, likely in the accretion disk. They suggested that the apparent energy shifts could reflect contributions from different Fe charge states at different times during the burst. Similar processes could be at work in 4U 1820. We note that there is also the strong Lyα transition of Ne X at 1.022 keV that is in the relevant energy range, and there are several observational indications for Ne overabundances in some ultracompact binaries (Juett & Chakrabarty 2003; Strohmayer 2004). Based on this a detection of Ne in 4U 1820 would not appear to be particularly surprising. A possible scenario then is that the emission line could be produced via reprocessing (reflection) from the accretion disk, and the narrow line widths would then reflect Keplerian motions in the outer disk. Using an upper limit on the line width (HWHM) of $\sigma_E = 1.18 \times 70 = 82.6$ eV, we would obtain $\Delta E/E \approx v/c = 82.6/1000 = 0.0826$, which implies $R > 146\,GM/c^2 \approx 325$ km for a 1.5 $M_\odot$ neutron star, which is not too dissimilar from the inferred maximum extent of the photosphere during PRE. This also ignores any inclination effects.

A plausible physical interpretation for the absorption lines is that they are formed in the super-Eddington wind generated by the PRE bursts. Yu & Weinberg (2018) presented hydrodynamical simulations of such winds that include modern nuclear reaction networks to follow the time-dependent burning, and composition. They find that the convective burning mixes the heavy element ashes of helium burning to sufficiently low column depths such that the ashes are eventually ejected in the wind. The ashes comprise a number of heavy elements, including; ^{48}Cr, ^{40}Ca, ^{44}Ti, ^{56}Ni, ^{36}Ar, ^{32}S, and ^{52}Fe. Among our detected absorption line energies, we find that for the highest energy line near 3 keV there are relatively few strong line candidates among those elements listed above. A plausible identification could be the He-like lines of S XV at 2.8839, 3.0325, and 3.1013 keV (van Hoof 2018), with one or more of these transitions being redshifted or blueshifted to the appropriate observed energy. We discuss likely sources of such shifts below. For the other absorption feature, at about 1.6–1.7 keV we note that there are plausible lines associated with several charge states of Fe, including Fe XXIII, XXIV, and XXV, as well as Cr XXIV, at about the right energy. Additionally, lines of Mg XI also fall in the appropriate range.

Alternatively, the apparent consistent energy shift between burst pairs 1 and 2 of all three spectral features seems to argue for a common origin, so we briefly comment on possible origins for the 1 keV emission line in the burst-driven wind as well. As noted by Yu & Weinberg (2018) in their

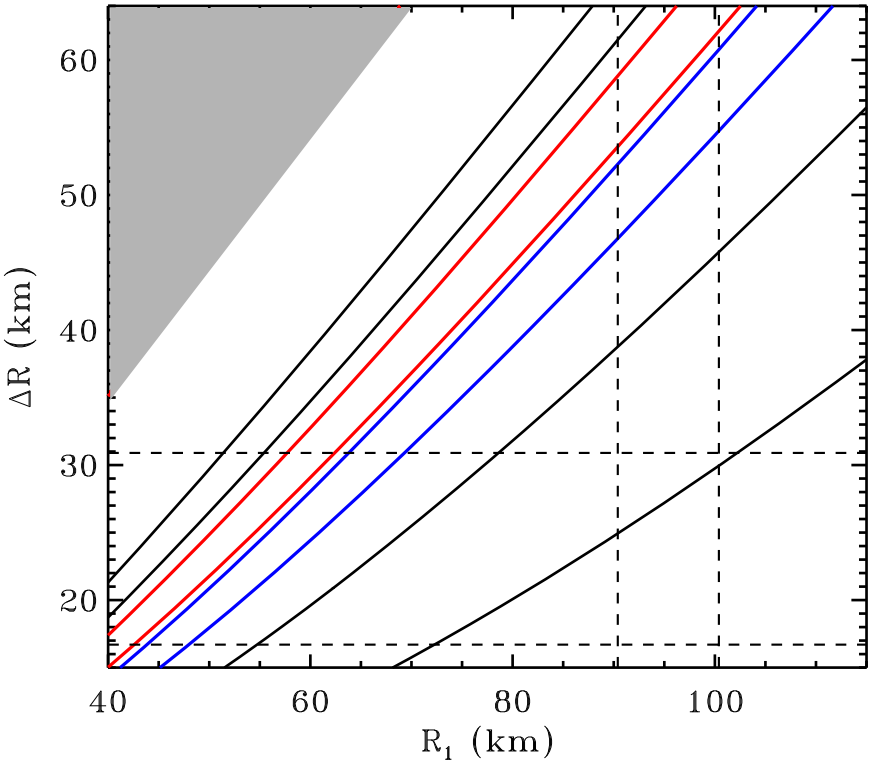

Figure 9. Contours of constant gravitational redshift, expressed as an observed energy ratio, E_1/E_2, are plotted vs. R_1 and $\Delta R = R_1 - R_2$. Here, R_1 and R_2 ($R_1 > R_2$) are two radial sites of photon emission with the same rest-frame energy. Contours of constant line ratio consistent with our measured value of 1.046 ± 0.006 are shown for neutron star masses of 1.5 (red) and 2.0 (blue) $M_\odot$. From bottom to top the black curves correspond to line ratios of 1.01, 1.02, 1.06, and 1.08 (for a neutron star mass of 1.5 $M_\odot$). Ignore the gray shaded region, as values were not computed there. The vertical and horizontal dashed lines mark representative ranges of the photospheric radii R_1 and ΔR derived from coadded spectra of burst pairs 1 and 2 (see Section 2.3).

hydrodynamical simulations, the base of the wind is initially at a relatively low column depth, so light (unburned) elements are launched first into the wind. As the burst progresses the base of the wind moves to greater column depths, eventually ejecting the burned ashes. Thus, composition gradients are likely to exist in the ejected wind, and perhaps emission lines could be formed in the outer parts of the wind. Another process that can form emission lines is resonant scattering (in't Zand et al. 2015), and it could be that conditions are favorable for this process to occur at some locations in the wind, such as, perhaps, in the Ne X Lyα line. More detailed theoretical calculations of radiative transfer in such burst-driven winds will be needed to explore these issues further.

A difficulty with making more precise line identifications, in addition to the need for higher spectral resolution, is the fact that both redshifts and blueshifts may be present, potentially with different contributions in the different bursts. Considering the gravitational redshift first, our spectral modeling indicates that between burst pair 1 and 2 there was an inferred variation in the average photospheric radius of $\approx$25 km. The difference in gravitational redshift between photons with the same rest-frame energy emitted at two different radii R_1 and R_2, expressed as the ratio of their observed energies, can be written as

$$\frac{E_1}{E_2} = \frac{(1 - 2GM/c^2R_1)^{1/2}}{(1 - 2GM/c^2R_2)^{1/2}}, \quad (1)$$

where E_1 and E_2 are the observed energies of photons emitted from radii R_1 and R_2, respectively. While the continuum spectroscopy discussed above provides good evidence that the average radial location of the photosphere is different between burst pairs 1 and 2, it is likely that these values do not accurately reflect the true emission radii (Suleimanov et al. 2011). Nevertheless, if the derived radii are representative, then the observed shifts are in the correct direction, that is, the line energies for burst pair 1, with a greater photospheric radius, are higher (less redshifted) than those for pair 2, with a smaller inferred radius.

Furthermore, we can explore the assumption that *all* of the observed shift is due to a gravitational redshift and see what that implies for the possible values of R_1 and R_2. Figure 9 shows contours of constant line ratio, E_1/E_2, as a function of R_1 and $\Delta R = R_1 - R_2$, for 1.5 (red) and 2.0 (blue) $M_\odot$ neutron stars. The red and blue contours enclose the 1σ range of our measured line ratios for 1.5 and 2.0 $M_\odot$ stars, respectively. The vertical and horizontal dashed lines show representative ranges ($\pm 1\sigma$) for R_1 and ΔR, based on the inferred photospheric radii estimated from the coadded spectra of burst pairs 1 and 2. If the estimated radii are at least approximately correct, then it would appear unlikely that all of the observed shift is due to gravitational effects alone, although we note that a heavier neutron star can more easily account for the observed shift.

Another likely culprit to induce blueshifts is the wind velocity itself. Wind velocity estimates from Yu & Weinberg (2018) suggest that the velocity is always $<0.01c$, which would limit a wind-induced line ratio, $s_w < 1.01$. Such estimates typically ignore radiative effects such as line-driving of the wind; if these are not significant, it would also appear that not all of the observed shift can be attributed to the wind. However, again an apparent shift due to this process would be in the

correct direction. The stronger PRE bursts (pair 1) would be expected to have the stronger wind, and thus stronger blueshifts and higher line energies, compared to pair 2, as observed. Since both of the above processes are likely present, and work in the same direction, it seems plausible that the observed shifts are produced by a combination of both effects acting together. With the present data it appears difficult to disentangle them; however, if correlated variations in the inferred photospheric radius and line energies with time could be accurately tracked in individual bursts, then it might be possible to independently determine the gravitational redshift.

4. Summary

We have presented strong evidence of the presence of narrow absorption and emission lines in *NICER* observations of the PRE phases of X-ray bursts from 4U 1820. We find an emission line near 1 keV, and absorption features near 1.7 and 3 keV. A significant, systematic shift in the line energies between pairs of bursts with different PRE strength is strongly indicative of a real physical effect associated with the bursts, and is likely produced by a combination of gravitational redshift and Doppler blueshifts associated with the burst-driven wind. It appears plausible that all of the features are produced in the PRE wind, but reprocessing (reflection) from the accretion disk could perhaps account for the 1 keV emission line. Based on theoretical modeling of the likely composition of the PRE-generated wind, we can tentatively identify the 3 keV absorption feature with the He-like lines of S XV. The *NICER* data suggest a wealth of information could be gleaned from such bursts by future observations. For example, *NICER* observations of a longer intermediate-duration burst or superburst could perhaps track variations in the line energies as the photosphere expands, providing a way to "see" the gravitational redshift directly. In addition, future, larger collecting area instruments, such as *Strobe-X*, *Athena* and *eXTP* (Barcons et al. 2017; in't Zand et al. 2019; Ray et al. 2019), with the ability to observe with higher throughput and/or better spectral resolution, could provide new tools to enable more precise line identifications and perhaps use such line detections to measure the compactness of the neutron star.

This work was supported by NASA through the *NICER* mission and the Astrophysics Explorers Program. This research also made use of data and software provided by the High Energy Astrophysics Science Archive Research Center (HEASARC), which is a service of the Astrophysics Science Division at NASA/GSFC and the High Energy Astrophysics Division of the Smithsonian Astrophysical Observatory. D.A. acknowledges support from the Royal Society. S.G. acknowledges the support of the Centre National d'Etudes Spatiales (CNES). G.K.J. acknowledges support from the Marie Skłodowska-Curie Actions grant No. 713683 (H2020; COFUNDPostdocDTU).

Facilities: NICER, ADS, HEASARC.

Software: NICERDAS (v 004), XSPEC (Arnaud 1996).

ORCID iDs

T. E. Strohmayer https://orcid.org/0000-0001-7681-5845
D. Altamirano https://orcid.org/0000-0002-3422-0074
D. Chakrabarty https://orcid.org/0000-0001-8804-8946
J. Chenevez https://orcid.org/0000-0002-4397-8370
A. C. Fabian https://orcid.org/0000-0002-9378-4072
S. Guillot https://orcid.org/0000-0002-6449-106X
G. K. Jaisawal https://orcid.org/0000-0002-6789-2723
R. M. Ludlam https://orcid.org/0000-0002-8961-939X
S. Mahmoodifar https://orcid.org/0000-0003-2386-1359
Christian Malacaria https://orcid.org/0000-0002-0380-0041

References

Arnaud, K. A. 1996, in ASP Conf. Ser. 101, Astronomical Data Analysis Software and Systems V, ed. G. H. Jacoby & J. Barnes (San Francisco, CA: ASP)
Ballantyne, D. R., & Strohmayer, T. E. 2004, ApJL, 602, L105
Barcons, X., Barret, D., Decourchelle, A., et al. 2017, AN, 338, 153
Barrière, N. M., Krivonos, R., Tomsick, J. A., et al. 2015, ApJ, 799, 123
Bildsten, L. 1995, ApJ, 438, 852
Cottam, J., Paerels, F., & Mendez, M. 2002, Natur, 420, 51
Cumming, A. 2003, ApJ, 595, 1077
Degenaar, N., Miller, J. M., Wijnands, R., Altamirano, D., & Fabian, A. C. 2013, ApJL, 767, L37
Fragile, P. C., Ballantyne, D. R., Maccarone, T. J., & Witry, J. W. L. 2018, ApJL, 867, L28
Galloway, D. K., & Keek, L. 2017, arXiv:1712.06227
Galloway, D. K., Lin, J., Chakrabarty, D., & Hartman, J. M. 2010, ApJL, 711, L148
Gendreau, K. C., Arzoumanian, Z., & Okajima, T. 2012, Proc. SPIE, 8443, 844313
Grindlay, J., Gursky, H., Schnopper, H., et al. 1976, ApJL, 205, L127
Güver, T., Özel, F., Marshall, H., et al. 2016, ApJ, 829, 48
Güver, T., Wroblewski, P., Camarota, L., & Özel, F. 2010, ApJ, 719, 1807
Haberl, F., Stella, L., White, N. E., Priedhorsky, W. C., & Gottwald, M. 1987, ApJ, 314, 266
in't Zand, J. J. M., Altamirano, D., Ballantyne, D. R., et al. 2015, arXiv:1501.02776
in't Zand, J. J. M., Bozzo, E., Qu, J., et al. 2019, SCPMA, 62, 29506
in't Zand, J. J. M., Homan, J., Keek, L., & Palmer, D. M. 2012, A&A, 547, A47
in't Zand, J. J. M., Strohmayer, T. E., Markwardt, C. B., & Swank, J. 2003, A&A, 409, 659
in't Zand, J. J. M., & Weinberg, N. N. 2010, A&A, 520, A81
Juett, A. M., & Chakrabarty, D. 2003, ApJ, 599, 498
Kajava, J. J. E., Nättilä, J., Poutanen, J., et al. 2017, MNRAS, 464, L6
Keek, L., Arzoumanian, Z., Chakrabarty, D., et al. 2018, ApJL, 856, L37
Keek, L., Ballantyne, D. R., Kuulkers, E., & Strohmayer, T. E. 2014a, ApJ, 789, 121
Keek, L., Ballantyne, D. R., Kuulkers, E., & Strohmayer, T. E. 2014b, ApJL, 797, L23
Lewin, W. H. G., van Paradijs, J., & Taam, R. E. 1993, SSRv, 62, 223
Li, Z., Suleimanov, V. F., Poutanen, J., et al. 2018, ApJ, 866, 53
Lin, J., Özel, F., Chakrabarty, D., & Psaltis, D. 2010, ApJ, 723, 1053
Ludlam, R. M., Miller, J. M., Arzoumanian, Z., et al. 2018, ApJL, 858, L5
Magnier, E., Lewin, W. H. G., van Paradijs, J., et al. 1989, MNRAS, 237, 729
Nakamura, N., Inoue, H., & Tanaka, Y. 1988, PASJ, 40, 209
Nättilä, J., Miller, M. C., Steiner, A. W., et al. 2017, A&A, 608, A31
Özel, F. 2006, Natur, 441, 1115
Rappaport, S., Nelson, L. A., Ma, C. P., & Joss, P. C. 1987, ApJ, 322, 842
Rauch, T., Suleimanov, V., & Werner, K. 2008, A&A, 490, 1127
Ray, P. S., Arzoumanian, Z., Ballantyne, D., et al. 2019, arXiv:1903.03035
Steiner, A. W., Lattimer, J. M., & Brown, E. F. 2010, ApJ, 722, 33
Strohmayer, T., & Bildsten, L. 2006, in Compact Stellar X-ray Sources, ed. W. H. G. Lewin & M. van der Klis (Cambridge: Cambridge Univ. Press), 113
Strohmayer, T. E. 2004, ApJL, 608, L53
Strohmayer, T. E., Arzoumanian, Z., Bogdanov, S., et al. 2018, ApJL, 858, L13
Strohmayer, T. E., & Brown, E. F. 2002, ApJ, 566, 1045
Suleimanov, V., Poutanen, J., & Werner, K. 2011, A&A, 527, A139
van Hoof, P. A. M. 2018, Galax, 6, 63
Villarreal, A. R., & Strohmayer, T. E. 2004, ApJL, 614, L121
Waki, I., Inoue, H., Koyama, K., et al. 1984, PASJ, 36, 819
Weinberg, N. N., Bildsten, L., & Schatz, H. 2006, ApJ, 639, 1018
Yu, H., & Weinberg, N. N. 2018, ApJ, 863, 53
Życki, P. T., Done, C., & Smith, D. A. 1999, MNRAS, 309, 561